RSC Advances

PAPER

View Article Online
View Journal | View Issue

Cite this: *RSC Adv.*, 2024, **14**, 7684

Synthesis, biological activities, and evaluation molecular docking-dynamics studies of new phenylisoxazole quinoxalin-2-amine hybrids as potential α-amylase and α-glucosidase inhibitors†

Siti Nurshahira Mohd Radzuan,[a] Lacksany Phongphane,[a] Mohamad Hafizi Abu Bakar,[b] Mohammad Tasyriq Che Omar,[c] Nor Shafiqah Nor Shahril,[b] Unang Supratman,[d] Desi Harneti,[d] Habibah A. Wahab[e] and Mohamad Nurul Azmi *[a]

New phenylisoxazole quinoxalin-2-amine hybrids **5a–i** were successfully synthesised with yields of 53–85% and characterised with various spectroscopy methods. The synthesised hybrids underwent *in vitro* α-amylase and α-glucosidase inhibitory assays, with acarbose as the positive control. Through the biological study, compound **5h** exhibits the highest α-amylase inhibitory activity with $IC_{50} = 16.4 \pm 0.1$ μM while compounds **5a–c**, **5e** and **5h** exhibit great potential as α-glucosidase inhibitors, with **5c** being the most potent ($IC_{50} = 15.2 \pm 0.3$ μM). Among the compounds, **5h** exhibits potential as a dual inhibitor for both α-amylase ($IC_{50} = 16.4 \pm 0.1$ μM) and α-glucosidase ($IC_{50} = 31.6 \pm 0.4$ μM) enzymes. Through the molecular docking studies, the inhibition potential of the selected compounds is supported. Compound **5h** showed important interactions with α-amylase enzyme active sites and exhibited the highest binding energy of -8.9 ± 0.10 kcal mol^{-1}, while compound **5c** exhibited the highest binding energy of -9.0 ± 0.20 kcal mol^{-1} by forming important interactions with the α-glucosidase enzyme active sites. The molecular dynamics study showed that the selected compounds exhibited relative stability when binding with α-amylase and α-glucosidase enzymes. Additionally, compound **5h** demonstrated a similar pattern of motion and mechanism of action as the commercially available miglitol.

Received 18th December 2023
Accepted 28th February 2024

DOI: 10.1039/d3ra08642a

rsc.li/rsc-advances

1. Introduction

Diabetes mellitus, commonly known as diabetes, is a metabolic disorder caused by the defects of insulin production, insulin secretion, or both.[1] Chronic cases of diabetes are often associated with long-term complications, dysfunction, or damage of internal organs.[1] Generally, diabetes cases are often categorized into two types: type 1 and type 2 diabetes (T2DM). T2DM is the most common type of diabetes, where it accounts for around 90% of all diabetes patients.[2] Due to the heterogeneous nature and inconsistency of patient response to the different T2DM medications, the care and treatment approach of this disease can be complex. The main medical treatments for T2DM include metformin, a first line T2DM drug, as well as sulfonylureas, DPP-4 inhibitors, GLP-1 receptor agonists, meglitinides, α-amylase inhibitors and α-glucosidase inhibitors.[3]

Nitrogen-containing aromatic heterocyclic compounds have been researched to have great applications in various fields. Quinoxaline is a type of aromatic heterocyclic compound, with its structure composed of a benzene ring and a pyrazine ring condensed together.[4,5] Quinoxaline derivatives have been researched to have numerous biological activities including antituberculosis, antibacterial, anticancer, anti-inflammatory, anti-malarial and anti-hyperglycaemic activities.[5] Quinoxaline derivatives exhibit great potential as T2DM treatment which includes DPP-4 inhibitors, GLP-1 receptor agonists, PPARγ and SUR agonists, α-amylase inhibitors, and α-glucosidase inhibitors.[4–11] In addition, isoxazoles are a class of azoles, with their structure containing a nitrogen and an oxygen atom in a five-membered aromatic ring.[12] This class of compound has been proven to play an important role in medicinal chemistry,

[a]*School of Chemical Sciences, Universiti Sains Malaysia, 11800 Minden, Penang, Malaysia. E-mail: shiraradzuan@gmail.com; lacksany.phongphane@gmail.com*

[b]*Bioprocess Technology Division, School of Industrial Technology, Universiti Sains Malaysia, 11800 Minden, Penang, Malaysia. E-mail: mhafizi88@usm.my; shafiqah17@gmail.com*

[c]*Biological Section, School of Distance Education, Universiti Sains Malaysia, 11800 Minden, Penang, Malaysia. E-mail: mtasyriq@usm.my*

[d]*Department of Chemistry, Faculty of Mathematics and Natural Sciences, Universitas Padjadjaran, 45363 Jatinangor, Indonesia. E-mail: unang.supratman@unpad.ac.id; desi.harneti@unpad.ac.id*

[e]*School of Pharmaceutical Sciences, Universiti Sains Malaysia, 11800 Minden, Penang, Malaysia. E-mail: habibahw@usm.my*

† Electronic supplementary information (ESI) available. See DOI: https://doi.org/10.1039/d3ra08642a

exhibiting great biological activity as antimicrobial, antibacterial, antiviral, anticancer, anti-inflammatory and antidiabetic agents.[13] As T2DM treatments, isoxazoles can be seen as a major component for various types of T2DM drugs such as protein tyrosine phosphatase 1B (PTP1B) inhibitors, GPR40 agonists, as well as α-amylase and α-glucosidase inhibitors.[12–17]

α-Glucosidase inhibitors are a type of digestive enzyme inhibitor for T2DM treatment that works to inhibit the glucosidase enzyme complexes, which are important for the digestion of carbohydrates. The inhibition of these enzymes causes a delay in carbohydrate absorption, which leads to the reduction of postprandial hyperglycaemia and lower blood glucose levels.[18] Meanwhile, α-amylase inhibitors are also a type of digestive enzyme inhibitor, which inhibits the α-amylase enzymes in charge of breaking down dietary carbohydrates. These inhibitors, however, are less common compared to α-glucosidase inhibitors.[19] Fig. 1 shows the structures of some quinoxaline and isoxazole-containing compounds that have been reported to have the potential as α-glucosidase and α-amylase inhibitors.[8,10,11,16,17] Through this, we can observe the potential of the hybridisation of quinoxaline and isoxazole groups to synthesise potent α-glucosidase and α-amylase inhibitors.

Some of the approved α-glucosidase and α-amylase inhibitors clinically used include acarbose, voglibose and miglitol, where they mainly inhibit α-glucosidase enzymes and only weakly inhibit α-amylase enzymes.[20] Generally, the side effects of these drugs can vary by patient and can include abdominal pain, diarrhoea, bloating, fluctuance, nausea and constipation. Compared to other T2DM treatments, this class of treatment still has a limit of usage for monotherapy due to its low efficacy and is in need of more research. Hence, taking the factors of the obvious potential of quinoxaline and isoxazole moieties towards the research for the treatment of T2DM, the lack of choice as well as the adverse side effects of this type of inhibitors into consideration, new quinoxaline–isoxazole derivatives are synthesised and evaluated for their α-amylase and α-glucosidase inhibitory activities. Through these biological studies, the quinoxaline–isoxazole derivatives show mild to outstanding potential as antidiabetic agents when compared to acarbose, and the inhibitory activities of these compounds are further confirmed with molecular docking and dynamic studies.

2. Results and discussion

2.1 Chemistry

The quinoxaline–isoxazole derivatives (**5a–i**) were synthesised *via* a 5-step reaction involving different reactions with several substituents, as illustrated in Scheme 1. The details of the synthesised compounds are depicted in the ESI.† All the reported compounds (**5a–i**) were synthesised in satisfactory to good yields (53 to 85%) and were characterised by spectroscopic methods including ^{1}H-NMR, ^{13}C-NMR, FTIR and HRMS analysis.

Compound **5a** exhibits peaks at 3431, 3088, 2978, 1531, and 1195 cm^{-1} of FTIR spectrum corresponding to the peaks of NH stretching, aromatic C–H stretching, C–H stretching for –CH_2CH_3, C=N stretching for isoxazole and quinoxaline groups, and C–O stretching for isoxazole group.

In the ^{1}H-NMR spectrum of compound **5a**, a total of 18 protons were integrated within the range of 1.24–7.75 ppm. A downfield singlet peak at 6.73 ppm corresponds to proton H-4′ attached to the isoxazole group. The integrated singlet peak for the two protons at H-6′ can be seen at 5.70 ppm, while the broad peak at 5.41 ppm corresponds to the NH-9 proton, with one proton integration. In the upfield region, a multiplet peak with 2 proton integration at the 3.66–3.58 ppm range was assigned to the protons at H-2, and a triplet peak at 1.33 ppm (J = 7.2 Hz) with 3 proton integration corresponds to the C–H_3 protons at H-11. The ^{13}C-NMR was also examined, and the structure of the compound is further confirmed. Within the 14.6–167.5 ppm range, a total of 20 carbon signals were observed. The signals for the quaternary and aromatic carbons are expected to be within the 167.5–124.1 ppm range. A carbon signal at 102.8

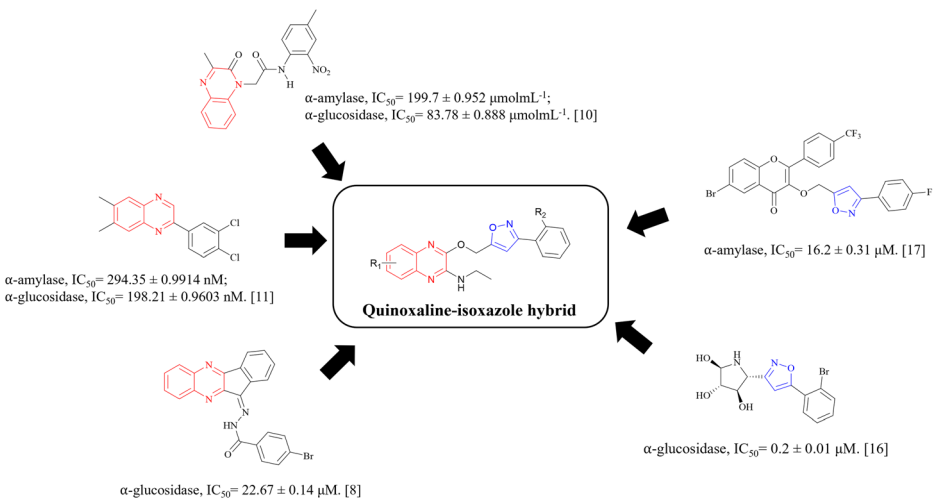

Fig. 1 Structures of potential α-glucosidase and α-amylase inhibitors bearing quinoxaline and isoxazole groups.

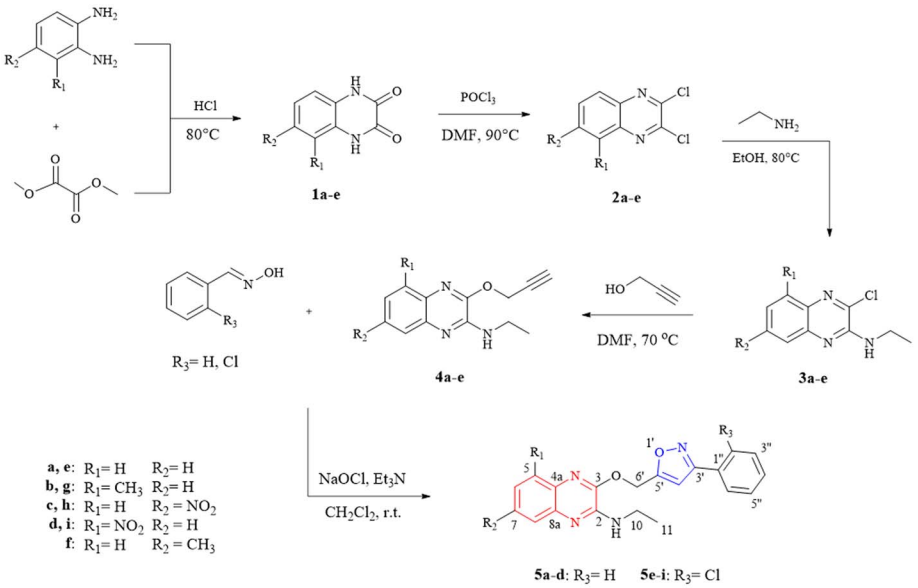

Scheme 1 Synthetic pathway of quinoxaline–isoxazole derivatives **5a–i**.

Table 1 *In vitro* α-amylase and α-glucosidase inhibitory potential of compounds **5a–i**

	IC_{50} (μM)	
Compound	α-Amylase	α-Glucosidase
5a	>125	41.9 ± 0.78
5b	>125	46.6 ± 0.1
5c	>125	15.2 ± 0.3
5d	>125	54.9 ± 0.9
5e	121.2 ± 1.4	42.8 ± 0.2
5f	42.1 ± 0.2	>125
5g	>125	>125
5h	16.4 ± 0.1	31.6 ± 0.4
5i	34.4 ± 0.36	66.9 ± 0.5
Acarbose	24.0 ± 0.9	49.3 ± 1.1

Table 2 Binding energy of related quinoxaline–isoxazole derivatives and acarbose with α-amylase and α-glucosidase enzymes

Enzyme	Compound	Binding energy[a] (kcal mol^{-1})
α-Amylase (2QV4)	**5h**	−8.9 ± 0.10
	5i	−8.6 ± 0.11
	Acarbose	−7.7 ± 0.11
α-Glucosidase (3TOP)	**5a**	−8.6 ± 0.15
	5b	−8.6 ± 0.10
	5c	−9.0 ± 0.20
	5e	−8.6 ± 0.10
	5h	−8.7 ± 0.15
	Acarbose	−7.5 ± 0.00

[a] SD for $n = 3$ experiments.

corresponds to carbon C-4′ in the isoxazole group. The signals 58.2 and 35.7 ppm in the upfield region are assigned to carbons at C-6′ and C-10 respectively, while the remaining signal at 14.7 ppm corresponds to the CH_3 carbon at C-11. The structure of the compound was further confirmed by running DEPT-135, COSY and HMBC NMR spectroscopy. The regioselectivity of the synthesis of compounds **3a–e**, **4a–e** and **5a–i** were also determined by previously reported literatures[21,22] and was further confirmed with X-ray previously reported crystallography data.[21]

2.2 Biology

All synthesised quinoxaline–isoxazole derivatives (**5a–i**) were tested for their *in vitro* α-amylase and α-glucosidase inhibitory activity. Fig. S68 and S69† visualises the graphs of inhibitory activity of the compounds with α-amylase and α-glucosidase enzymes respectively. The probability of the compounds to be toxic at certain concentrations may cause the curve to deviate in a concentration-dependent manner and not follow the dose–response curve following a phenomenon termed as hormesis.[23,24] Table 1 demonstrates the inhibitory potential of the compounds against α-amylase and α-glucosidase activity with their calculated IC_{50} values. For α-amylase, compound **5h** displayed the most significant inhibitory potential (IC_{50} = 16.4 ± 0.1 μM) compared to acarbose (IC_{50} = 24.0 ± 0.9 μM). Compound **5i** also exhibits good inhibitory activity (IC_{50} = 34.4 ± 0.36 μM) comparable to acarbose. As for α-glucosidase enzyme, compounds **5a–c**, **5e** and **5h** exhibits significant inhibitory potential. Compound **5c** in particular, exhibits the highest inhibitory potential (IC_{50} = 15.2 ± 0.3 μM) compared to acarbose (IC_{50} = 49.3 ± 1.1 μM). The rest of the compounds also exhibit great potential, with IC_{50} values in the range of 31.6–46.6 μM. Furthermore, from the IC_{50} values calculated, it can be observed that compound **5h** exhibits potential as both α-amylase and α-glucosidase inhibitors, in comparison to acarbose. The compound which exhibits the greatest α-amylase

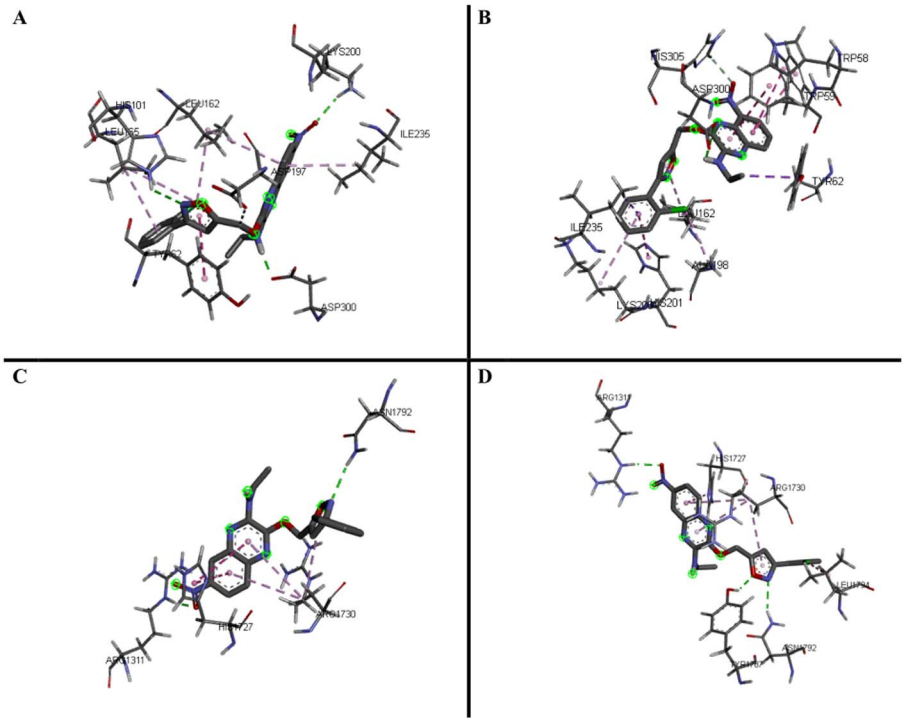

Fig. 2 3D predicted binding modes of compounds **5h** (A) and **5i** (B) with modelled α-amylase and compounds **5c** (C) and **5h** (D) with modelled α-glucosidase (CtMGAM).

inhibitory activity and 2nd highest α-glucosidase activity, can be deduced to have the potential as a dual inhibitor.

2.3 Molecular docking study

Through the α-amylase and α-glucosidase inhibition assays performed on the quinoxaline–isoxazole derivatives, several potent compounds were selected for molecular docking analysis. The molecular docking analysis was done by using the crystal structures of the human pancreatic α-amylase complexed with nitrite and acarbose (PDB ID: 2QV4)[25] and the C-terminal of human maltase glucoamylase (CtMGAM, α-glucosidase) complexed with acarbose (PDB ID: 3TOP)[26] as reference complexes for the docking process. The MGAM protein is a type of α-glucosidase enzyme that is in charge of hydrolysing sugars

Table 3 Key binding interactions of compounds **5h** and **5i** with α-amylase protein

Protein	Compound	Protein residue	Interaction unit of compounds	Type of interaction
α-Amylase (2QV4)	**5h**	ASP300	NH of amide	H-Bond
		HIS101	N of isoxazole	H-Bond
		LYS200	NO_2	H-Bond
		ASP197	CH_2	Carbon H-bond
		TYR62	Isoxazole	π–π stacked
		LEU162	Quinoxaline, –Cl	π–alkyl
		LEU165	Phenyl, quinoxaline	π–alkyl
		ILE235	NH of amide	π–alkyl
	5i	ASP300	NH of amide	H-Bond
		HIS305	NO_2	Carbon H-bond
		ILE235	Phenyl	π–sigma
		TYR62	CH_2CH_3	π–sigma
		HIS201	Phenyl	π–π T-shaped/π–π stacked
		TRP58	Quinoxaline	π–π T-shaped/π–π stacked
		TRP59	Quinoxaline	π–π T-shaped/π–π stacked
		ALA198	–Cl	π–alkyl/alkyl
		LYS200	Phenyl	π–alkyl/alkyl
		LEU162	Isoxazole	π–alkyl/alkyl
			–Cl	π–alkyl/alkyl

Table 4 Key binding interactions of compounds **5c** and **5h** with α-glucosidase protein

Protein	Compound	Protein residue	Interaction unit of compounds	Type of interaction
α-Glucosidase (3TOP)	**5c**	ARG1311	$-NO_2$	H-Bond
		ASN1792	N of isoxazole	H-Bond
		ARG1730	Quinoxaline, isoxazole	π–alkyl
	5h	ARG1311	$-NO_2$	H-Bond
		ASN1792	O of isoxazole	Carbon H-bond
		ARG1311	Phenyl	π–alkyl
		TYR1787	O of isoxazole	H-Bond
		HIS1727	Quinoxaline	π–π T-shaped
		LEU1794	–Cl	π–alkyl
		ARG1730	Quinoxaline, isoxazole	π–alkyl

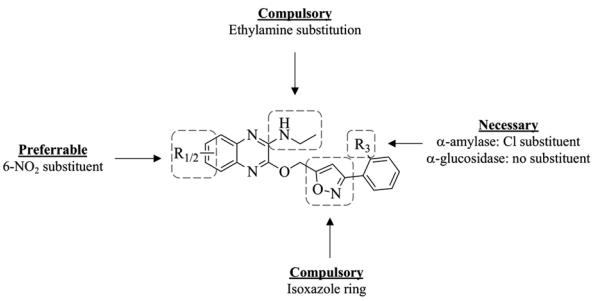

Fig. 3 SAR study of quinoxaline–isoxazole compounds.

like oligosaccharides and maltose into glucose, which makes them vital in production of glucose for human beings.[26] The C-terminal MGAM (PDB ID: 3TOP) is selected as the docking protein for α-glucosidase as it has been reported to be preferred in inhibition with acarbose, compared to the N-terminal.[26] This is also supported by our previous study reported by Phongphane *et al.* in 2023.[27] The molecular docking results of the selected quinoxaline–isoxazole compounds and acarbose are indicated *via* binding energy with targeted enzymes and are tabulated in Table 2.

With α-amylase, compounds **5h** and **5i** were selected to perform docking analysis, and it can be observed that both compounds exhibit higher binding energy with enzyme compared to acarbose (-7.7 ± 0.11 kcal mol^{-1}). Compound **5h** exhibits the highest binding energy of -8.9 ± 0.10 kcal mol^{-1} and forms hydrogen bonds with amide group (ASP300), nitrogen atom of isoxazole (HIS101), and NO_2 substituent (LYS200). With the quinoxaline group, two π–alkyl bonds were formed with LEU162 and ILE235. More π–alkyl bonds were formed between the phenyl group with protein residue LEU165 and Cl substituent respectively with proteins LEU162 and LEU165. A π–π stacked interaction was also formed between the isoxazole group and TYR62 residue.

For compound **5i**, similar bond interactions are also seen between ASP300 residue with the amide group to form a hydrogen bond, residues TRP58 and TRP59 with quinoxaline group to form π–π stacked, as well as an π–alkyl bond formed between the isoxazole group and residue LEU162. The three-dimensional (3-D) binding interaction of these compounds with the active site of α-amylase is exhibited in Fig. 2A and B. From the docking performed, it can be said that the presence of the quinoxaline, isoxazole and amide groups are essential, whereas the type of substituent, such as the –Cl substituent, also plays a great role in increasing the binding energy of the compounds with the target protein, α-amylase. The details of the binding interactions of these compounds with α-amylase have been tabulated in Table 3.

For α-glucosidase enzyme, five of the most potent inhibitors (**5a–c**, **5e**, and **5h**) were selected based on their IC_{50} values, and all the compounds exhibit higher binding energy when compared to acarbose (-7.5 ± 0.00 kcal mol^{-1}). Among the five compounds, **5c** exhibits the highest binding energy (-9.0 ± 0.20 kcal mol^{-1}), followed by **5h** (-8.7 ± 0.15 kcal mol^{-1}). Both compounds exhibit hydrogen bond interactions, with the bonds in **5c** forming *via* the nitro substituent (ARG1311) and the nitrogen atom of isoxazole (ASN1792), while for **5h**, the bonds formed *via* the oxygen atom (TYR1787) and the nitrogen atom (ASN1792) of the isoxazole group. The rest of the interactions in compound **5c** include the π–π T-shaped bond forming *via* the quinoxaline group (HIS1727) as well as π–alkyl interactions with the quinoxaline and isoxazole group with protein residue ARG1730.

In **5h**, similar interactions are also observed, with π–π T-shaped interaction forming *via* the quinoxaline group (HIS1727). Three π–alkyl bonds were also formed *via* the Cl substitution at the phenyl group (LEU1794), the quinoxaline and isoxazole group (ARG1730), and the phenyl group (ARG1311). The three-dimensional (3-D) binding interaction of these compounds with the active site of α-glucosidase (CtMGAM) is exhibited in Fig. 2C and D and the details of the binding interactions of the selected compounds with α-glucosidase have been tabulated in Table 4. From this analysis, it can be said that the presence of the quinoxaline and isoxazole groups are necessary, while the presence of certain substituents such as chloro and nitro substituents also play an important role to achieve high binding energy with the target protein, α-glucosidase.

2.4 Structure–activity relationship (SAR)

The SAR studies of the *in vitro* tested compounds **5a–i** were done by considering the types and positions of the substituents in the

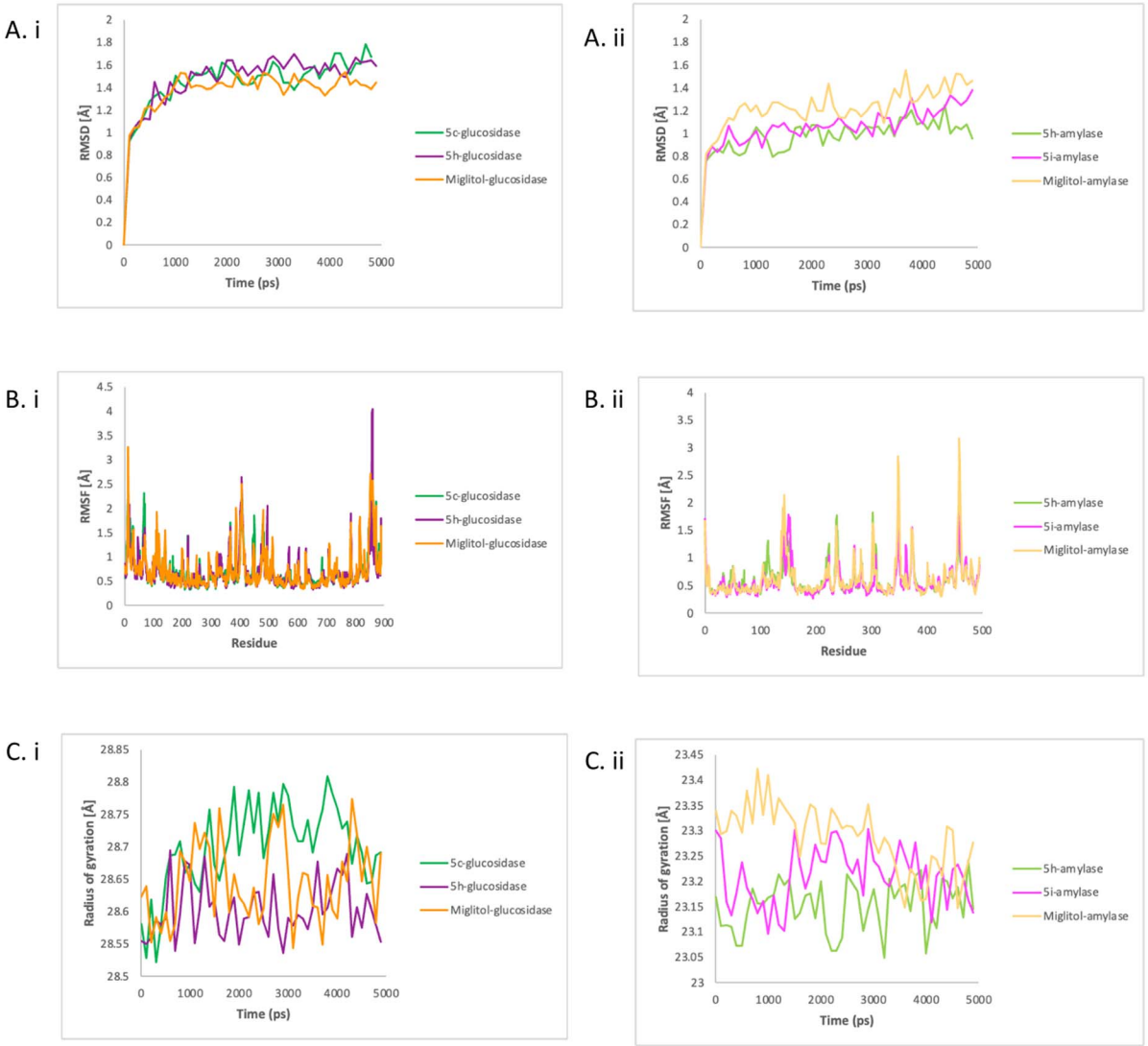

Fig. 4 The RMSD (A), RMSF (B) and R_g (C) of glucosidase with compounds **5c**, **5h**, and miglitol (i) and amylase with compounds **5h**, **5i**, and miglitol (ii).

compounds and their potential as α-amylase and α-glucosidase inhibitors. For α-amylase inhibition, the compounds with unsubstituted R_3 site (**5a–d**) display weaker inhibitory activity when compared to compounds with chloro substitution at R_3 (**5e–i**) and acarbose. Through this, it can be concluded that the presence of Cl substituent as an electronegative atom at site R_3 is necessary to achieve higher α-amylase inhibitory potential. This can be further solidified by the *in silico* molecular docking studies, where the Cl substituent is observed to form multiple interaction bonds such as π–alkyl and alkyl bonds with the enzyme.

From the binding energy of the compounds exhibited in the *in silico* study, it can be said that substitution at position C-7 may be essential to achieve greater α-amylase inhibitory activity compared to substitution at C-5. It can also be concluded that when the type of substituents at the quinoxaline moiety is compared, the compounds with nitro substituent exhibit the most potent α-amylase inhibitory activity. These trends can be observed with the comparison of compounds **5h** and **5i**; **5h** exhibits the greatest α-amylase inhibitory potential among all the quinoxaline–isoxazole compounds synthesised, followed by **5i**, where both compounds are nitro substituted at C-7 (R_2) and C-5 (R_1) respectively.

As for α-glucosidase inhibition, among all the quinoxaline–isoxazole compounds synthesised, compound **5c** with nitro substitution at C-7 and unsubstituted R_3 site, exhibits the most potent inhibition activity ($IC_{50} = 15.2 \pm 0.3$ μM), enhanced to about three-folds, compared to acarbose ($IC_{50} = 49.3 \pm 1.1$ μM). However, when a nitro group is substituted at C-5 for compound **5d**, the inhibition activity decreased over 3 folds ($IC_{50} = 54.9 \pm 0.9$ μM). The same trend can be observed for compounds with chloro substitution at site R_3, where the inhibitory activity of compound **5h** ($IC_{50} = 31.6 \pm 0.4$ μM) bearing nitro substitution at C-7 was enhanced to two folds compared to its counterpart **5i**

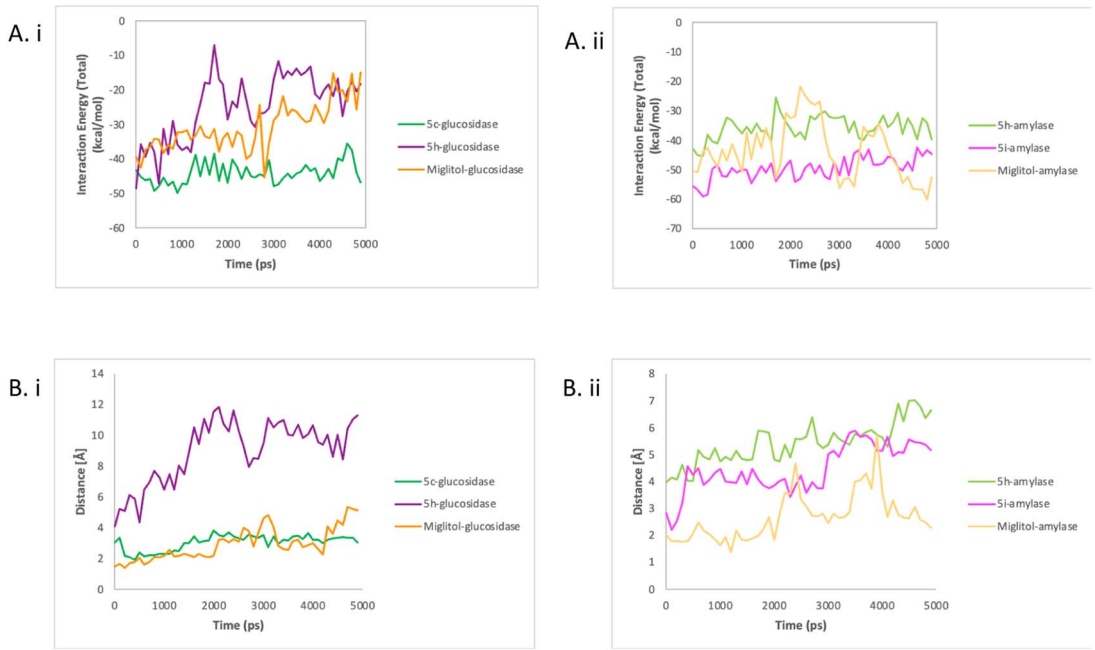

Fig. 5 The interaction energy (A) and enzyme–compound distance (B) of glucosidase with compounds **5c**, **5h**, and miglitol (i) and amylase with compounds **5h**, **5i**, and miglitol (ii).

(IC_{50} = 66.9 ± 0.5 μM) that bears a nitro substitution at C-5. From this, it can be concluded that among the nitro-substituted compounds synthesised, substitution at C-7 is favoured to produce greater α-glucosidase inhibitory potential compared to substitution at C-5. Moreover, it can be observed that overall, the unsubstituted R_3 compounds (**5a–d**) exhibit more potent α-glucosidase inhibitory activity compared to the chloro-substituted compounds (**5e–f**). For instance, compound **5c** exhibits a more potent α-glucosidase inhibitory activity compared to **5h**, where both compounds are nitro-substituted at C-7. The same can also be said for the other substituents: 5-CH_3 (**5b** and **5g**), 5-NO_2 (**5d** and **5i**) as well as the unsubstituted derivatives (**5a** and **5e**). These trends are further solidified by the *in silico* study conducted, where compound **5c** exhibited the highest binding energy, followed by **5h**, and compounds **5a**, **5b** and **5e**. From this overall analysis, it can be also concluded that compound **5h** exhibits a potential to act as dual inhibitors for both α-amylase and α-glucosidase enzymes. The summary of the SAR study of these compounds as potential α-amylase and α-glucosidase inhibitors is illustrated in Fig. 3.

2.5 Molecular dynamics study

The simulations of four enzyme–compound complexes (**5c**–glucosidase, **5h**–glucosidase, **5h**–amylase, **5i**–amylase) and two control enzyme–compound complexes (miglitol–glucosidase, and miglitol–amylase) were carried out with the Amber program for 5000 picoseconds. To evaluate the stability and dynamics of each complex, various analyses were performed on the resulting MD trajectories, including root mean square deviation (RMSD) profile, Cα root mean square fluctuation (RMSF), radius of gyration (R_g), interaction energy, binding free energy, and residue interaction, using the PyTraj and ProLIF tools integrated in a python notebook.[28,29]

2.5.1 Stability, residue fluctuations and enzyme forms. The stability of the complexes between **5c** and **5h** with glucosidase and **5h** and **5i** with amylase was analysed by generating RMSD profiles for the backbone residues over a time scale of 5000 ps. The results from Fig. 4Ai showed that the RMSD values for the three glucosidases were relatively stable, fluctuating between 1.3 and 1.8. The control, miglitol–glucosidase complex had the lowest RMSD values, indicating a close match to the reference set of values. The **5c**–glucosidase and **5h**–glucosidase complexes showed slightly higher RMSD values after 2500 ps, indicating a slight deviation from the reference set of values compared with the control. As shown in Fig. 4Aii, the RMSD values for the **5h**–amylase and **5i**–amylase were similar throughout the simulation and relatively stable.

In contrast with glucosidase, the miglitol–amylase had higher values, indicating a greater deviation from the reference set of values. All the systems showed a relatively stable in RMSD values over time, indicating a stable dynamics simulation between enzymes and compounds was achieved. To assess the flexibility and stiffness of different residues in amylase and glucosidase when complexed with compounds, RMSF plots were created from the simulation trajectories of the enzyme's dynamics. As shown in Fig. 4Bi, the highest fluctuations were detected in **5h**–glucosidase at residue SER1366, followed by miglitol–glucosidase also at residue SER1366 and **5c**–glucosidase at residue SER1440.

As shown in Fig. 4Bii, significant fluctuation patterns were observed in miglitol–amylase and **5i**–amylase, indicating restricted movement during the simulation. The greatest deviation in the Cα atom of PHE348 in miglitol–amylase was

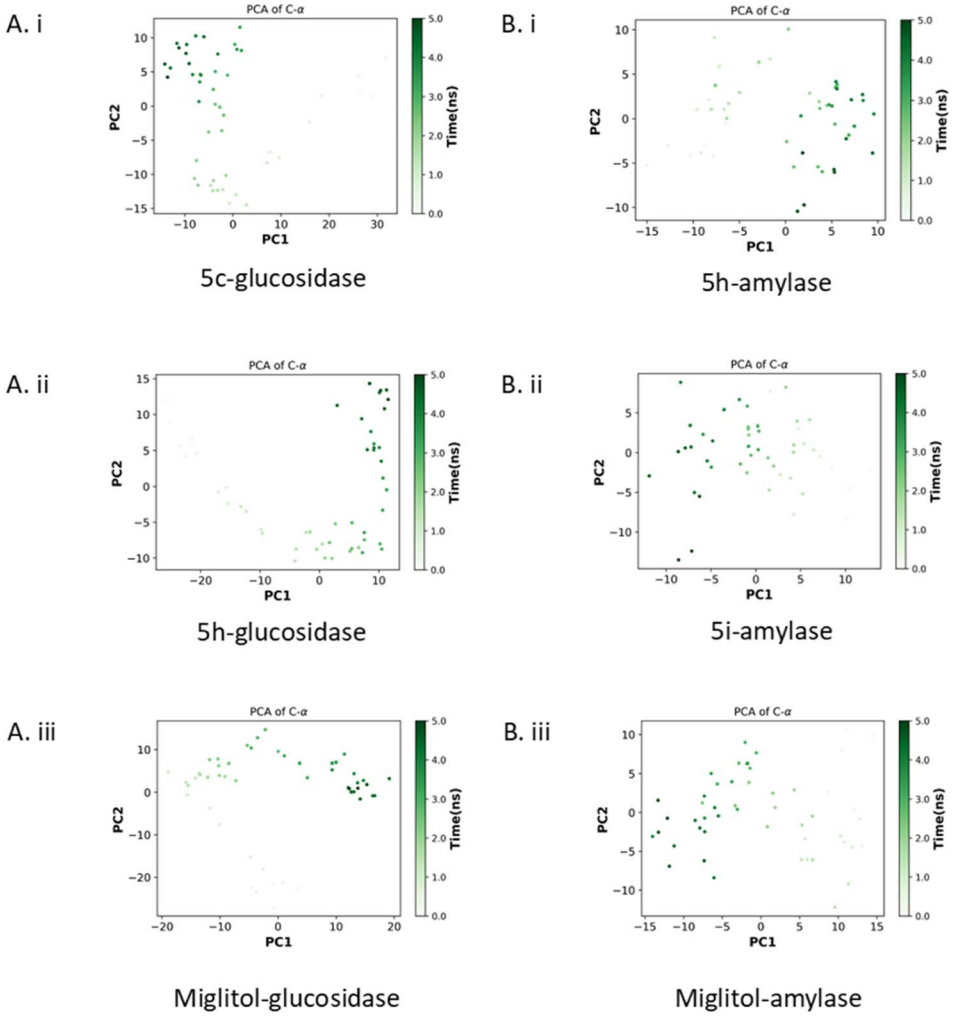

Fig. 6 The principal component analysis. Glucosidase with compounds **5c**, **5h**, and miglitol (Ai–iii) and amylase with compounds **5h**, **5i**, and miglitol (Bi–iii).

detected throughout the simulation, indicating that this residue was crucial for ligand binding. Binding with **5i** resulted in a greater deviation of the amylase residue ASP153 than the effect of **5h** binding on residue LEU237 and GLN302 in the Cα atom. In both enzymes, **5h** showed a similar fluctuation pattern with miglitol and might share the similar mode of action to miglitol. The compactness of both enzymes when bound with tested compounds and control was analysed by calculating the R_g values, which represent the square root of the average of the squared distances of the atoms or particles from the centre of mass. As shown in Fig. 4Ci, **5h**–glucosidase and miglitol–glucosidase had a relatively steady R_g value over time, with an average of 28.6 angstroms. However, **5c**–glucosidase had higher values on average (28.7 angstroms), indicating that it was becoming less compact when bound with **5c**. In contrast, Fig. 4Cii showed that after amylase was complexed with **5h**, **5i**, and miglitol, different R_g values were observed, indicating different levels of compactness. Despite this, there was a relatively similar average value observed from 3500 ps to the end of the simulation time. The decreasing values of the miglitol–amylase complex indicated that the amylase enzyme changed from rigid to less compact when bound with miglitol, while the size and shape of amylase enzymes remained stable when complexed with **5h** and **5i**. In glucosidase, **5h** showed a similar compactness pattern as miglitol while in amylase, **5i** showed a similar compactness pattern as miglitol.

2.5.2 Interaction energy and enzyme–compound distance. The strength of the interaction between enzyme and compound in a complex environment can be influenced by electrostatic energy and van der Waals energy that contribute to the total energy of a molecular system. The strength of a system can be analysed by examining the total energy value. As depicted in Fig. 5Ai, the binding of glucosidase with different compounds such as **5c**, **5h**, and miglitol demonstrated the various strength between the enzyme and these compounds. The interaction of glucosidase with **5c** was found to be the strongest, followed by miglitol and **5h**. This indicated that **5c** interacted more frequently with glucosidase compared to **5h** and the control. A similar pattern was observed in amylase, as shown in Fig. 5Aii. The average interaction energy of amylase with **5i** was found to

Table 5 Binding free energy and residues interaction of the **5c**–glucosidase, **5h**–glucosidase, and miglitol–glucosidase complexes

Complex	MM-GBSA Generalized Born (Δ total ± std. dev.)	Residues with interaction occur more 70% of frames	Type of interaction
5c–Glucosidase	−25.1252 ± 1.7469	TYR1618	Hydrophobic
		THR1621	Hydrophobic
		LEU1622	Hydrophobic
		LYS1625	Hydrophobic
		VAL1631	Hydrophobic
		PRO1658	Hydrophobic
		TYR1715	Hydrophobic
			π-Stacking
			Hydrophobic
		ALA1746	Hydrophobic
		GLY1747	Hydrophobic
		GLY1748	Hydrophobic
		TRP1749	π-Stacking
5h–Glucosidase	−15.7285 ± 6.4800	TYR1251	Hydrophobic
			π-Stacking
		TRP1355	Hydrophobic
			π-Stacking
			Hydrophobic
		ASP1368	Hydrophobic
		TRP1369	π-Stacking
			Hydrophobic
			Hydrophobic
		ASP1370	Hydrophobic
		GLN1372	Hydrophobic
		PHE1427	Hydrophobic
		PHE1559	π-Stacking
		PHE1560	
Miglitol–glucosidase	−14.6832 ± 4.1961	PHE1289	Hydrophobic
		THR1290	Hydrophobic
		PRO1329	Hydrophobic
		GLU1400	Hydrophobic
		ASN1404	Hydrophobic
		PRO1405	H-Bond
		GLN1406	Hydrophobic
		ARG1410	Hydrophobic
			H-Bond

be the strongest (−49.5), followed by miglitol (−43.6) and **5h** (−35.7). This showed that **5i** formed a high number of nonbonded interaction with amylase compared to **5h** and the control. These results indicated that **5c** interacted favourably with glucosidase and **5i** was found to interact strongly with amylase, and both compounds might be comparable and slightly superior to the control, miglitol.

These findings also proved that nonbonded interactions are important in compound–enzyme interaction and stability as previously reported.[30] The positioning of the compounds in the active site of enzymes was one of the key factors that led to a strong interaction energy. As shown in Fig. 5Bi, there was a short average distance of 2 angstroms observed between miglitol and the residues in the active site of glucosidase. The distance between **5c** and residues in the active site was only slightly higher, with an average of 3 angstroms. On the other hand, longer distances ranging from 4 to 12 angstroms were recorded between **5h** and the active site residues. A similar trend was seen in amylase, as shown in Fig. 5Bii, with initially short distances between miglitol and the active site residues, but with higher distances observed after 2000 ps reaching up to 5 angstroms. Unlike glucosidase, **5i** maintained a stable distance of 4.5 angstroms. As for **5h**, it displayed longer distances with the active site residues, which ranged from 4 to 7 angstroms. These findings support the impact of compound position on the interaction energy between enzymes and compounds.

2.5.3 Principal component analysis. The dynamics trajectories were utilized to measure the variation in movement between the control miglitol–enzyme complex and the compound–enzyme complex. The results of the principal component analysis (PCA) revealed that the enzyme underwent overall expansion during the simulation, thus the principal components (PCs) significantly contributed to the global motion of the enzyme. The two-directional movements of the PCs were analysed as the first eigenvector (PC1) and second

Table 6 Binding free energy and residues interaction of the **5h**–amylase, **5i**–amylase, and miglitol–amylase complexes

Complex	MM-GBSA Generalized Born (Δ total ± std. dev.)	Residues with interaction occur more 70% of frames	Type of interaction
5h–Amylase	−23.1177 ± 2.5202	PRO54	Hydrophobic
		TRP58	Hydrophobic
			π-Stacking
		TRP59	Hydrophobic
			π-Stacking
		TYR62	Hydrophobic
		GLN63	Hydrophobic
		ALA106	Hydrophobic
		VAL107	Hydrophobic
		SER108	H-Bond
		THR163	Hydrophobic
		LEU165	Hydrophobic
5i–Amylase	−28.8653 ± 2.0533	TRP58	Hydrophobic
		TRP59	Hydrophobic
			π-Stacking
			π–Cation
		TYR62	Hydrophobic
		GLN63	Hydrophobic
		TYR151	Hydrophobic
			π-Stacking
		LEU162	Hydrophobic
		THR163	Hydrophobic
		LEU165	Hydrophobic
		ASP197	Hydrophobic
		ALA198	Hydrophobic
		LYS200	Hydrophobic
		HIS201	Hydrophobic
			π-Stacking
		ILE235	Hydrophobic
		HIS299	Hydrophobic
		ASP300	Hydrophobic
		HIS305	Hydrophobic
			π-Stacking
Miglitol–amylase	−22.2484 ± 7.9166	ARG267	H-Bond
			Hydrophobic
		ASN301	H-Bond
			Hydrophobic
		GLN302	Hydrophobic
		ARG303	Hydrophobic
		GLY304	Hydrophobic
		GLY309	Hydrophobic
		ALA310	Hydrophobic
		ILE312	Hydrophobic
		THR314	Hydrophobic
		TRP316	Hydrophobic
		ASP317	H-Bond
			Hydrophobic
		ARG346	H-Bond
		PHE348	Hydrophobic

eigenvector (PC2). As depicted in Fig. 6Ai–iii, the eigenvalues for **5c**–glucosidase ranged from 30 to −15 for PC1 and from −15 to 12 for PC2. The **5h**–glucosidase complex exhibited eigenvalues from −30 to 12 for PC1 and from −12 to 15 for PC2. The eigenvalues for the miglitol bound glucosidase were from −18 to 20 for PC1 and from −30 to 18 for PC2.

As shown in Fig. 6Bi–iii, the eigenvalues of the **5h**–amylase complex fluctuated between −13 to 10 for PC1 and −10 to 10 for PC2. Meanwhile, the **5i**–amylase complex had eigenvalues ranging from 14 to −12 for PC1 and −14 to 10 for PC2. The miglitol-bound glucosidase had eigenvalues that ranged from 13 to −14 for PC1 and −13 to 10 for PC2. The PCA results indicated that the binding of the compounds to glucosidase

created stable enzyme–compound complexes. The **5h**–glucosidase complex showed a similar pattern of motion to the miglitol–glucosidase complex, especially at the end of the simulation, while the **5c**–glucosidase complex showed an opposing motion. However, all glucosidase complexes were very stable and occupied the least phase space compared to the amylase complexes. Additionally, the **5i**–amylase complex showed a similar pattern of motion to the miglitol–amylase complex, suggesting that the compound may have the same mechanism of action as miglitol.

2.5.4 Binding energy and interaction residue analysis. The calculation of binding energy was performed using the MM-GBSA approach (which combines molecular mechanics [MM], generalized Born [GB], and surface area [SA]). The two-end-state method employed in this calculation determines the binding free energy of the system by only considering the initial conformations of the enzyme and compound and the final conformation of the complex throughout the simulation runs.

The binding free energy values for the complexes of **5c**–glucosidase, **5h**–glucosidase, and miglitol–glucosidase are displayed in Table 5. The **5c**–glucosidase complex had the lowest binding free energy at -25.13 kcal mol^{-1}, followed by **5h**–glucosidase complex with -15.73 kcal mol^{-1}, and miglitol–glucosidase complex with -14.68 kcal mol^{-1}. Analysis of the simulation revealed the interactions that occurred in more than 70% of frames. For the **5c**–glucosidase complex, five residues showed interaction as displayed in molecular docking, with the exception of TRP1749's hydrogen bond. Additionally, six other residues formed hydrophobic interactions. A similar pattern was observed in the **5h**–glucosidase complex where five residues maintained their hydrophobic interactions, except for LYS1460, and four other residues generated additional hydrophobic interactions. The 5000 ps trajectories analysis showed that both the **5c**–glucosidase and **5h**–glucosidase complexes mainly formed hydrophobic interactions and π-stacking.

On the other hand, the miglitol–glucosidase complex formed both hydrophobic interactions and hydrogen bonds. The depiction of the binding free energy of **5h**–amylase, **5i**–amylase, and miglitol–amylase complexes are shown in Table 6. The binding free energy value was recorded as -23.12 kcal mol^{-1} for the **5h**–amylase complex, -28.87 kcal mol^{-1} for the **5i**–amylase complex, and -22.25 kcal mol^{-1} for the miglitol–amylase complex. Out of the three compounds, **5i** showed the lowest total binding free energy value. The simulation analysis revealed that interactions occurred in more than 70% of frames. In the **5h**–amylase complex, seven residues that demonstrated interaction as presented in the molecular docking were maintained in the simulation, except for the hydrogen bond of residue THR163 which was replaced with a hydrophobic interaction. Furthermore, a hydrogen bond was formed at SER108, and hydrophobic interactions were formed by two adjacent residues. A similar pattern was observed in the **5i**–amylase complex. Eight residues maintained their hydrophobic interactions as shown in the molecular docking. However, ASP300 and HIS305 formed a hydrophobic interaction instead of a hydrogen bond as demonstrated by molecular docking. Additional hydrophobic interactions were generated by four adjacent residues. Similar to glucosidase, 5000 ps of trajectories analysis showed that both **5h**–amylase and **5i**–amylase complexes mostly formed hydrophobic interactions and π-stacking. In contrast, the miglitol–glucosidase complex formed hydrophobic interactions and hydrogen bonds.

3. Conclusion

To summarise, new quinoxaline–isoxazole hybrids **5a–i** were successfully synthesised with moderate to high yield of range 53–85%. The synthesised compounds underwent *in vitro* α-amylase and α-glucosidase inhibitory assays, and several compounds exhibit potential. Compound **5h**, bearing 6-NO_2 and 2-Cl substituents, exhibits the most potential as α-amylase inhibitor ($IC_{50} = 16.39 \pm 0.1$ μM) while compounds **5a–c**, **5e** and **5h** all exhibit potential as α-glucosidase inhibitor, in which compound **5c**, bearing 6-NO_2 substituent, is the most potent inhibitor with $IC_{50} = 15.15 \pm 0.3$ μM. From this, it can be observed that compound **5h** exhibits the potential to act as dual inhibitors for both α-amylase and α-glucosidase enzymes. Based on the SAR studies conducted, nitro substitution at C-6 ($R_{1/2}$) is the most preferred substituent to achieve the most potent inhibitory activity for both enzymes, while the substitution at R_3 varies between enzymes. Chloro substitution at site R_3 is only necessary to achieve more potent α-amylase inhibitory activity, while unsubstituted R_3 compounds exhibit more potent inhibitory activity for α-glucosidase. The molecular docking and dynamic studies conducted also further confirm the inhibitory activity of the selected compounds, where compound **5h** exhibited the greatest binding energy of -8.9 ± 0.10 kcal mol^{-1} with α-amylase, while compound **5c** exhibited the greatest binding energy of -9.0 ± 0.20 kcal mol^{-1} with α-glucosidase. The molecular dynamics study revealed that the selected compounds displayed relative stability when binding with α-amylase and α-glucosidase enzymes. The formation of hydrophobic interactions between the compounds and residues within the active site of enzymes played a role in influencing the enzyme's compactness and affinity. In addition, **5h** exhibited a comparable pattern of motion and mechanism of action to the commercially available miglitol inhibitor. Overall, compound **5h** exhibits promising potential as dual inhibitor for α-amylase and α-glucosidase enzymes and serve as the steppingstone towards the research for more effective T2DM treatments.

4. Materials and methods

4.1 Chemistry

All chemicals and materials purchased from Sigma Aldrich Co. and Merck Chemical Co. and used without purification. DMF and DCM solvents were dried over 4 Å molecular sieves. The purification of synthesised compounds *via* column chromatography was performed using Merck silica gel (0.040–0.063 mm), while the thin-layer chromatography (TLC) was performed using silica-coated aluminium sheets (silica gel 60 F_{254}) and the chromatograms were visualized under UV 254–366 nm Fourier-Transform Infrared (FTIR) spectra were obtained using a PerkinElmer 2000 FTIR Spectrum spectrometer (PerkinElmer,

Waltham, MA, USA). The nuclear magnetic resonance (NMR) spectra were obtained using 500 MHz Bruker Advance NMR (500 MHz for ^{1}H-NMR, 125 MHz for ^{13}C-NMR) spectrometer system and the data was analysed using Topspin 4.1.4 software (Bruker Bioscience, Billerica, MA, USA). The chemical shifts were internally calibrated using the residual DMSO peak (^{1}H: 2.50 ppm, ^{13}C: 39.5 ppm), the $CDCl_3$ peak (^{1}H: 7.26 ppm, ^{13}C: 77.0 ppm) or the tetramethylsilane (TMS) signal at 0.00 ppm for both ^{1}H and ^{13}C-NMR. The high-resolution mass spectroscopy (HRMS) was recorded by Waters Xevo QTOF MS (Milford, Massachusetts, United States), and reported in *m*/*z*. The synthesis method for the intermediates, as well as the NMR, FTIR and HRSM spectra of all synthesised compounds are presented in ESI.†

4.1.1 Synthesis of quinoxaline derivatives. The synthesis of quinoxaline derivatives (**1a–4f**) was initiated with the reaction of 1,2-diaminobenzene with dimethyl oxalate to synthesise quinoxaline-2,3-diones **1a–f**.[31] Then, compounds **1a–f** were reacted with $POCl_3$ to form 2,3-dichloroquinoxalines **2a–f**,[31] which is then reacted with ethylamine in ethanol to produce 3-chloro-*N*-ethylquinoxalin-2-amines **3a–f**.[32] Compounds **3a–f** were then reacted with propargyl alcohol in the presence of potassium *tert*-butoxide in DMF to produce *N*-ethyl-3-(prop-2-yn-1-yloxy)quinoxalin-2-amine **4a–f**.[33] To synthesise final target compounds **5a–i**, **4a–f** were reacted with benzaldehyde oxime derivatives in the presence of Et_3N and $NaOCl_3$.[34] The crude products were extracted and further purified *via* column chromatography to afford pure compounds with 53–85% yield. All synthesised compounds were characterised with NMR, FTIR and HRMS spectroscopy.

4.1.2 General procedure for the synthesis of *N*-ethyl-3-((3-phenylisoxazol-5-yl)methoxy)quinoxalin-2-amine derivatives (5a–i). Compounds **5a–i** were synthesised by stirring respective compounds **4** (1.2 eq.) with 6% NaOCl in the presence of Et_3N at 0 °C. After 5 min, benzaldehyde oxime (1.0 eq.) in DCM was added into the mixture and the reaction was stirred for 2 hours. After 2 hours, the reaction was left to stir at room temperature and monitored using TLC. After completion, the mixture was extracted and evaporated, and the crude obtained was purified by gravitational column chromatography to produce final products **5a–i**.

*4.1.2.1 N-Ethyl-3-((3-phenylisoxazol-5-yl)methoxy)quinoxalin-2-amine (**5a**).* IR (neat) ν: 3431 (m, N–H), 3088 (w, aromatic C–H), 2978 (w, Csp_3–H), 1531 (s, aromatic C=C), 1447 (s, C=N), 1378 (m, C–N), 1195 (s, C–O); ^{1}H-NMR (500 MHz, $CDCl_3$) δ: 7.80–7.82 (m, 2H), 7.68 (d, J = 8.0 Hz, 2H), 7.44–7.47 (m, 4H), 7.31–7.34 (m, 1H), 6.73 (s, 1H), 5.70 (s, 2H), 5.41 (s), 3.58–3.66 (m, 2H), 1.33 (t, J = 7.2 Hz, 3H); ^{13}C-NMR (125 MHz, $CDCl_3$) δ: 167.5, 162.7, 146.9, 144.4, 139.6, 134.4, 130.2, 129.0, 129.0, 128.7, 127.1, 126.9, 126.9, 126.4, 125.5, 124.1, 102.8, 58.2, 35.7, 14.7; HRMS (+ESI) $[M + H]^+$: 347.1504, $C_{20}H_{19}N_4O_2$, requires 347.1508.

*4.1.2.2 N-Ethyl-5-methyl-3-((3-phenylisoxazol-5-yl)methoxy)quinoxalin-2-amine (**5b**).* IR (neat) ν: 3445 (m, N–H), 3062 (w, aromatic C–H), 2963 (w, Csp_2–H), 2826 (w, Csp_3–H), 1529 (s, aromatic C=C), 1476 (m, C=N), 1298 (m, C–N), 1203 (s, C–O); ^{1}H-NMR (500 MHz, $CDCl_3$) δ: 7.80–7.82 (m, 2H), 7.54 (d, J = 7.6 Hz, 1H), 7.45–7.46 (m, 3H), 7.31 (d, J = 7.6 Hz, 1H), 7.23 (t, J = 7.6 Hz, 1H), 6.76 (s, 1H), 5.73 (s, 2H), 5.44 (s, 1H), 3.65–3.72 (m, 2H), 2.67 (s, 3H), 1.38 (t, J = 7.2, 3H); ^{13}C-NMR (125 MHz, $CDCl_3$) δ: 167.7, 162.7, 146.6, 143.4, 138.3, 134.3, 133.8, 130.2, 128.9, 128.9, 128.7, 127.4, 126.9, 124.2, 123.7, 102.7, 58.0, 35.7, 17.4, 14.5; HRMS (+ESI) $[M + H]^+$: 361.1678, $C_{21}H_{21}N_4O_2$, requires 361.1650.

*4.1.2.3 N-Ethyl-7-nitro-3-((3-phenylisoxazol-5-yl)methoxy)quinoxalin-2-amine (**5c**).* IR (neat) ν: 3379 (w, N–H), 3057 (w, aromatic C–H), 2926 (w, Csp_3–H), 1579 (s, aromatic C=C), 1546 (s, NO_2), 1502 (m, C=N), 1327 (m, =C–N), 1201 (s, C–O); ^{1}H-NMR (500 MHz, $CDCl_3$) δ: 8.57 (d, J = 2.5 Hz, 1H), 8.25 (dd, J = 9.0, 2.5 Hz, 1H), 7.80–7.82 (m, 2H), 7.68 (d, J = 9.0 Hz, 1H), 7.46–7.47 (m, 3H), 6.78 (s, 1H), 5.84 (s, 1H), 5.72 (s, 2H), 3.64–3.69 (m, 2H), 1.35 (t, J = 7.2 Hz, 3H); ^{13}C-NMR (125 MHz, $CDCl_3$) δ: 166.5, 162.8, 148.1, 145.8, 144.4, 143.6, 133.4, 130.3, 129.1, 128.5, 127.4, 126.9, 126.3, 125.9, 122.7, 121.7, 103.3, 58.5, 35.9, 14.4; HRMS (+ESI) $[M + H]^+$: 392.1357, $C_{20}H_{18}N_5O_4$, requires 392.1359.

*4.1.2.4 N-Ethyl-5-nitro-3-((3-phenylisoxazol-5-yl)methoxy)quinoxalin-2-amine (**5d**).* IR (neat) ν: 3414 (w, N–H), 3067 (aromatic C–H), 2932 (w, Csp_3–H), 1529 (s, NO_2), 1297 (m, C–N), 1189 (s, C–O); ^{1}H-NMR (500 MHz, $CDCl_3$) δ: 7.79–7.84 (m, 4H), 7.45–7.46 (m, 3H), 7.31 (t, J = 8.0 Hz, 1H), 6.72 (s, 1H), 5.77 (s, 1H), 5.70 (s, 2H), 3.59–3.62 (m, 2H), 1.30 (t, J = 7.2 Hz, 3H); ^{13}C-NMR (125 MHz, $CDCl_3$) δ: 171.3, 166.8, 162.8, 147.6, 145.3, 135.6, 132.7, 130.5, 130.4, 129.1, 128.6, 126.9, 122.3, 122.0, 103.1, 60.5, 58.7, 36.1, 14.4; HRMS (+ESI) $[M + H]^+$: 392.1354, $C_{20}H_{18}N_5O_4$, requires 392.1359.

*4.1.2.5 3-((3-(2-Chlorophenyl)isoxazol-5-yl)methoxy)-N-ethylquinoxalin-2-amine (**5e**).* IR (neat) ν: 3441 (w, N–H), 3064 (w, aromatic C–H), 2974 (w, Csp_3–H), 1531 (s, aromatic C=C), 1442 (m, C=N), 1309 (m, C–N), 1196 (m, C–O), 759 (m, Cl); ^{1}H-NMR (500 MHz, $CDCl_3$) δ: 7.74 (dd, J = 7.5, 1.8 Hz, 1H), 7.65–7.69 (m, 2H), 7.50 (dd, J = 7.5, 1.8 Hz, 1H), 7.30–7.45 (m, 4H), 6.92 (s, 1H), 5.71 (s, 2H), 5.43 (s, 1H), 3.57–3.66 (m, 2H), 1.33 (t, J = 7.2 Hz, 3H); ^{13}C-NMR (125 MHz, $CDCl_3$) δ: 166.7, 150.5, 147.6, 146.9, 139.6, 134.4, 132.9, 131.0, 130.5, 130.0, 128.8, 127.9, 127.0, 126.4, 125.4, 124.2, 106.2, 58.2, 35.7, 14.6; HRMS (+ESI) $[M + H]^+$: 381.1119, $C_{20}H_{18}ClN_4O_2$, requires 381.1118.

*4.1.2.6 3-((3-(2-Chlorophenyl)isoxazol-5-yl)methoxy)-N-ethyl-7-methylquinoxalin-2-amine (**5f**).* IR (neat) ν: 3451 (w, N–H), 3056 (aromatic C–H), 2967 (w, Csp_2–H), 2928 (w, Csp_3–H), 1592 (m, aromatic C=C), 1530 (s, C=N), 1317 (m, C–N), 1200 (m, C–O), 763 (m, Cl); ^{1}H-NMR (500 MHz, $CDCl_3$) δ 7.76 (dd, J = 7.6, 1.7 Hz, 1H, H-5), 7.54–7.57 (m, 1H, H-3″), 7.45–7.50 (m, 2H), 7.34–7.41 (m, 2H, H-7), 7.14 (dd, J = 7.5, 1.7 Hz, 1H), 6.91 (s, 1H′), 5.69 (s, 2H), 5.39 (br. s, 1H), 3.58–3.64 (m, 2H), 2.49 (s, 3H), 1.34 (t, J = 7.2 Hz, 3H); ^{13}C-NMR (125 MHz, $CDCl_3$) δ: 166.8, 161.3, 146.5, 144.4, 139.5, 137.1, 132.9, 132.4, 131.1, 130.5, 128.7, 128.0, 127.2, 125.9, 125.8, 125.1, 106.2, 58.1, 35.6, 21.5, 14.7 (C-11); HRMS (+ESI) $[M + H]^+$: 395.1274, $C_{21}H_{20}ClN_4O_2$, requires 395.1275.

*4.1.2.7 3-((3-(2-Chlorophenyl)isoxazol-5-yl)methoxy)-N-ethyl-5-methylquinoxalin-2-amine (**5g**).* IR (neat) ν: 3445 w, (N–H), 3065 (w, aromatic C–H), 2967 (w, Csp_2–H), 2927 (w, Csp_3–H), 1529 (s, aromatic C=C), 1298 (m, C–N), 1203 (m, C–O), 762 (m, Cl); ^{1}H-

NMR (500 MHz, $CDCl_3$) δ: 7.73 (dd, J = 7.9, 1.8 Hz, 1H), 7.52 (d, J = 7.9 Hz, 1H), 7.49 (dd, J = 7.9, 1.2 Hz, 1H), 7.34–7.41 (m, 2H, H-8), 7.30 (d, J = 7.9 Hz, 1H), 7.21 (t, J = 7.6 Hz, 1H), 6.91 (s, 1H, H-4′), 5.70 (s, 2H, H-6′), 5.40 (br. s, 1H, N–H), 3.61–3.66 (m, 2H, H-10), 2.62 (s, 3H), 1.34 (t, J = 7.2 Hz, 3H); ^{13}C-NMR (125 MHz, $CDCl_3$) δ: 166.9, 161.2, 146.6, 143.3, 138.3, 134.3, 133.8, 132.9, 131.0, 130.5, 128.0, 127.4, 127.2, 124.2, 123.7, 106.1, 58.0, 35.7, 17.4, 14.5; HRMS (+ESI) $[M + H]^+$: 395.1279, $C_{21}H_{20}ClN_4O_2$, requires 395.1275.

*4.1.2.8 3-((3-(2-Chlorophenyl)isoxazol-5-yl)methoxy)-N-ethyl-7-nitroquinoxalin-2-amine (**5h**).* IR (neat) ν: 3426 (w, N–H), 3065 (m, aromatic C–H), 2924 (m, Csp_3–H), 1544 (m, aromatic C=C), 1500 (C=N), 1459 (m, NO_2), 1325 (m, C–N), 1080 (m, C–O), 767 (m, Cl); ^{1}H-NMR (500 MHz, $CDCl_3$) δ: 8.57 (d, J = 2.5 Hz, 1H), 8.25 (dd, J = 9.0, 2.5 Hz, 1H), 7.74 (dd, J = 9.0, 2.5 Hz, 1H), 7.68 (d, J = 9.0 Hz, 1H), 7.51 (d, J = 9.0 Hz, 1H), 7.35–7.43 (m, 2H), 6.96 (s, 1H), 5.85 (s, 1H), 5.74 (s, 2H), 3.65–3.70 (m, 2H), 1.36 (t, J = 7.2, 3H); ^{13}C-NMR (125 MHz, $CDCl_3$) δ: 165.7, 161.3, 148.1, 145.8, 144.4, 143.6, 133.4, 132.9, 131.3, 130.9, 130.5, 127.7, 127.2, 125.9, 122.7, 121.6, 106.7, 58.6, 35.9, 14.4; HRMS (+ESI) $[M + H]^+$: 426.0959, $C_{20}H_{17}ClN_5O_4$, requires 426.0969.

*4.1.2.9 3-((3-(2-Chlorophenyl)isoxazol-5-yl)methoxy)-N-ethyl-5-nitroquinoxalin-2-amine (**5i**).* IR (neat) ν: 3327 (w, N–H), 3141 (s, aromatic C–H), 2923 (m, Csp_3–H), 1594 (m, aromatic C=C), 1532 (s, C=N), 1502 (s, NO_2), 1224 (m, C–N), 1032 (m, C–O), 767 (m, Cl); ^{1}H-NMR (500 MHz, $CDCl_3$) δ: 7.80–7.84 (m, 2H), 7.74 (dd, J = 7.5, 1.8 Hz, 1H), 7.50 (dd, J = 7.5, 1.8 Hz, 1H), 7.34–7.42 (m, 2H), 7.31 (t, J = 8.0 Hz, 1H) 6.92 (s, 1H), 5.77 (s, 1H), 5.72 (s, 2H), 3.60–3.66 (m, 2H), 1.32 (t, J = 7.2 Hz, 3H); ^{13}C-NMR (125 MHz, $CDCl_3$) δ: 165.9, 161.3, 147.5, 145.2, 135.5, 132.9, 132.6, 131.2, 131.0, 130.5, 130.4, 129.5, 127.8, 127.2, 122.2, 121.9, 106.4, 58.5, 35.9, 14.3; HRMS (+ESI) $[M + H]^+$: 426.0971, $C_{20}H_{17}ClN_5O_4$, requires 426.0969.

4.2 Biology

4.2.1 α-Amylase inhibitory assay. The α-amylase inhibition assay was conducted following the procedure reported by Abu Bakar *et al.*[35] with slight modifications. The α-amylase enzyme solution was prepared by dissolving 5.0 mg of enzyme in 20 mL of phosphate buffer (20.0 mM, pH 6.9). Firstly, 50 μL of enzyme solution was added into a set of tubes, along with 50 μL of compounds with 5 varying concentrations of range 7.8–125 μg mL^{-1}. The tubes were then preincubated at 37 °C for 20 min. After incubation, 50 μL of 1% starch solution was added into the sets of tubes and further incubated for 15 min. Then, 0.1 mL of 3,5-dinitrosalicylic acid (DNS) reagent was added to stop the reaction, and the tubes were immersed in a boiling hot water bath for 10 min. After 10 min, the tubes were cooled to room temperature and 1 mL of distilled water was added. The absorbance of the final products was measured at 540 nm with an MRP-96 microplate reader (Halo, Dynamica, Australia). The negative control was prepared using the same method, with the compounds replaced with the addition of buffer and acarbose was used as the positive control. The equation for the calculation of the percentage of inhibition is shown in the equation below:

$$\text{Percentage of inhibition } (\%) = \left(\frac{\text{Abs}_{\text{control}} - \text{Abs}_{\text{compound}}}{\text{Abs}_{\text{control}}}\right) \times 100$$

where $\text{Abs}_{\text{control}}$ represents the absorbance value of the control and $\text{Abs}_{\text{command}}$ represents the absorbance value of the compound. The IC_{50} values of each compound were calculated using the GraphPad Prism 9.0 software (GraphPad Software, La Jolla, CA).

4.2.2 α-Glucosidase inhibitory assay. The α-glucosidase inhibitory assay was conducted following the procedure reported by Abu Bakar *et al.*[35] with slight modifications. The α-glucosidase enzyme solution (1.0 U mL^{-1}) was prepared by weighing 0.1 mg of enzyme and dissolving it in 18.6 mL of phosphate buffer (20 mM, pH 6.9). Firstly, in a set of tubes, 100 μL of enzyme solution was added, followed by compounds with 5 varying concentrations of range 7.8–125 μg mL^{-1}. The tubes were incubated at 37 °C for 10 min. After incubation, 50 μL of 3.0 mM 4-nitrophenyl α-D-glucopyranoside (pNPG) solution was added as the substrate and the tubes were further incubated for 20 min at 37 °C. After the incubation period, 2 mL of 0.1 M sodium carbonate (Na_2CO_3) was added to stop the reaction. The sample mixtures were transferred into a microplate and the absorbance was measured using an MRP-96 microplate reader (Halo, Dynamica, Australia). The negative control was prepared using the same method, with the compound replaced with the addition of buffer and acarbose was used as the positive control. The equation for the calculation of the percentage of inhibition of α-glucosidase is shown in the equation below:

$$\text{Percentage of inhibition } (\%) = \left(\frac{\text{Abs}_{\text{control}} - \text{Abs}_{\text{compound}}}{\text{Abs}_{\text{control}}}\right) \times 100$$

where $\text{Abs}_{\text{control}}$ represents the absorbance value of the control and $\text{Abs}_{\text{command}}$ represents the absorbance value of the compound. The IC_{50} values of each compound were calculated using the GraphPad Prism 9.0 software (GraphPad Software, La Jolla, CA).

4.3 Molecular docking

Selected quinoxaline compounds were selected to perform molecular docking studies according to their potency as great enzyme inhibitors. For α-amylase enzyme, compounds **5h** and **5i**, while compounds **5a**, **5b**, **5c**, **5e**, and **5h** were selected to perform molecular docking studies with α-glucosidase enzyme. The molecular docking studies were performed according to the method reported by Mohamad *et al.*[36] Firstly, the compound structures were drawn using ChemDraw and converted to PDB format. The 3D structures of human pancreatic alpha-amylase complexed with nitrite and acarbose (α-amylase, PDB ID: 2QV4) and C-terminal of human Maltase-Glucoamylase (ctMGAM) complexed with acarbose (α-glucosidase, PDB ID: 3TOP) were fetched by ID *via* from the protein databank *via* the UCSF Chimera 1.14. The water molecules and unrelated heteroatoms were removed using the Dock Prep tool and further processed before docking commenced. To recognise the α-

amylase enzyme binding sites, the grid box parameters were set to 68, 81 and 77 Å along the *X*, *Y*, and *Z*-axis as grid size and 20, 62 and 16 Å along the *X*, *Y*, and *Z*-axes as the grid centre with 0.375 Å grid spacing. As for α-glucosidase, the grid box parameters were set to 127, 117 and 151 in grid size and −38, 11 and −13 in grid centre along the *X*, *Y*, and *Z*-axis respectively, with 0.375 Å in grid spacing. The docking was performed, and binding energies were calculated *via* the AutoDock Vina tool. The output results of the docking were further analysed and visualised in 2D and 3D *via* Discovery Studio Visualizer Client, 2020 (Dassault Systèmes BIOVIA, Discovery Studio Modeling Environment, Release 2017, San Diego: Dassault Systèmes, 2016).

4.4 Molecular dynamics

The molecular dynamics simulations for all the enzyme–compound complexes (**5c**–glucosidase, **5h**–glucosidase, **5h**–amylase, and **5i**–amylase) and controls (miglitol–glucosidase and miglitol–amylase) were performed using protein_ligand.ipynb[37] with the ff19SB force field. The Generalized AMBER Force Field 2 (GAFF2) was used for compounds as characterized using the Antechamber program. For each molecular simulation, the initial conformation for each complex was the docking pose generated from the docking protocol. The complex was solvated in an orthorhombic TIP3P water box (12 nm) with periodic boundary conditions and neutralized with 0.15 molar of NaCl using the AMBER tleap program. Prior to beginning the simulation, each complex was treated with an energy minimization consisting of 20 000 steps of steepest descent algorithm. Next, each molecular model was equilibrated for 1 ns in the isothermal–isobaric (NPT) ensemble (298 K and 1.01325 MPa) with position restraint force constant at 700 kJ mol^{-1}. Finally, the molecular dynamics simulations were carried out in the NPT ensemble (298 K) for 5000 ps with integration timestep of 2 fs. Structural analyses of MD simulation were done by using ProLIF and PyTraj tools integrated in protein_lignad.ipynb. The plots depicting the dynamics stabilities including root mean square deviation (RMSD), root mean square fluctuation (RMSF), radius of gyration (R_g), interaction energy, principal component analysis (PCA), binding free energy, and residue interaction of all systems were generated from the tools.

Author contributions

Conceptualization, M. N. A.; methodology, S. N. M. R., L. P., M. H. A. B., M. T. C. O. and M. N. A.; investigation, S. N. M. R., L. P., and M. T. C. O.; formal analysis, S. N. M. R., L. P., M. T. C. O., U. S., D. H., and N. S. N. S.; data curation, S. N. M. R. and L. P.; validation, M. N. A., M. H. A. B., M. T. C. O., U. S., D. H., and H. A. W.; resources, M. N. A., M. H. A. B., and U. S.; visualization, S. N. M. R., L. P., and M. T. C. O.; writing—original draft preparation, S. N. M. R., M. T. C. O. and M. N. A.; writing—review and editing, M. N. A., M. H. A. B. and M. T. C. O.; supervision, M. N. A., M. H. A. B. and M. T. C. O.; project administration, M. N. A.; funding acquisition, M. N. A. All authors have read and agreed to the published version of the manuscript.

Conflicts of interest

The authors declare no conflict of interest.

Acknowledgements

The authors would like to acknowledge the financial support from the Ministry of Higher Education Malaysia (MOHE) under Fundamental Grant Research Scheme (FRGS) – FRGS/1/2019/STG01/USM/01/2 and Graduate Excellence Programme (GrEP) MARA for S. N. M. R.

Notes and references

1 American Diabetes Association, *Diabetes Care*, 2014, **37**, S81–S90.
2 What is diabetes, **https://www.idf.org/aboutdiabetes/what-is-diabetes.html**, accessed December 2022.
3 D. M. Nathan, *Jama*, 2015, **314**, 1052–1062.
4 J. A. Pereira, A. M. Pessoa, M. N. D. Cordeiro, R. Fernandes, C. Prudêncio, J. P. Noronha and M. Vieira, *Eur. J. Med. Chem.*, 2015, **97**, 664–672.
5 S. Tariq, K. Somakala and M. Amir, *Eur. J. Med. Chem.*, 2018, **143**, 542–557.
6 M. K. Ibrahim, I. H. Eissa, A. E. Abdallah, A. M. Metwaly, M. M. Radwan and M. A. ElSohly, *Bioorg. Med. Chem.*, 2017, **25**, 1496–1513.
7 Y. M. Syam, M. M. Anwar, S. S. Abd El-Karim, S. A. Elseginy, B. M. Essa and T. M. Sakr, *RSC Adv.*, 2021, **11**, 36989–37010.
8 M. S. Khan, M. A. Munawar, M. Ashraf, U. Alam, A. Ata, A. M. Asiri, S. Kousar and M. A. Khan, *Bioorg. Med. Chem.*, 2014, **22**, 1195–1200.
9 T. Settypalli, V. R. Chunduri, A. K. Maddineni, N. Begari, R. Allagadda, P. Kotha and A. R. Chippada, *New J. Chem.*, 2019, **43**, 15435–15452.
10 M. Missioui, S. Mortada, W. Guerrab, G. Serdaroğlu, S. Kaya, J. T. Mague, E. M. Essassi, M. E. Faouzi and Y. Ramli, *J. Mol. Struct.*, 2021, **1239**, 130484, DOI: **10.1016/j.molstruc.2021.130484**.
11 S. Hameed, K. M. Khan, P. Taslimi, U. Salar, T. Taskin-Tok, D. Kisa, F. Saleem, M. Solangi, M. H. U. Ahmed and K. Rani, *Int. J. Biol. Macromol.*, 2022, **211**, 653–668.
12 F. Hu and M. Szostak, *Adv. Synth. Catal.*, 2015, **357**, 2583–2614.
13 A. Sysak and B. Obmińska-Mrukowicz, *Eur. J. Med. Chem.*, 2017, **137**, 292–309.
14 H. Zhao, G. Liu, Z. Xin, M. D. Serby, Z. Pei, B. G. Szczepankiewicz, P. J. Hajduk, C. Abad-Zapatero, C. W. Hutchins, T. H. Lubben and M. R. Jirousek, *Bioorg. Med. Chem. Lett.*, 2004, **14**, 5543–5546.
15 L. Yang, J. Zhang, L. Si, L. Han, B. Zhang, H. Ma, J. Xing, L. Zhao, J. Zhou and H. Zhang, *Eur. J. Med. Chem.*, 2016, **116**, 46–58.

16 C. K. Lin, L. W. Cheng, H. Y. Li, W. Y. Yun and W. C. Cheng, *Org. Biomol. Chem.*, 2015, **13**, 2100–2107.
17 I. Saidi, M. Manachou, M. Znati, J. Bouajila and H. B. Jannet, *J. Mol. Struct.*, 2022, **1247**, 131379, DOI: **10.1016/j.molstruc.2021.131379**.
18 J. J. Marín-Peñalver, I. Martín-Timón, C. Sevillano-Collantes and F. J. del Cañizo-Gómez, *World J. Diabetes*, 2016, **7**, 354, DOI: **10.4239/wjd.v7.i17.354**.
19 S. Kumar, S. Narwal, V. Kumar and O. Prakash, *Pharmacogn. Rev.*, 2011, **5**, 19, DOI: **10.4103/0973-7847.79096**.
20 A. Bedekar, K. Shah and M. Koffas, *Adv. Appl. Microbiol.*, 2010, **71**, 21–73.
21 Y. B. Lee, Y. D. Gong, H. Yoon, C. H. Ahn, M. K. Jeon and J. Y. Kong, *Bioorg. Med. Chem.*, 2010, **18**, 7966–7974.
22 P. V. Babu, S. Mukherjee, G. S. Deora, K. S. Chennubhotla, R. Medisetti, S. Yellanki, P. Kulkarni, S. Sripelly, K. V. Parsa, K. Chatti, K. Mukkanti and M. Pal, *Org. Biomol. Chem.*, 2013, **11**, 6680.
23 G. Nordberg, B. A. Fowler, M. Nordberg, D. B. Moffett, D. B. Mumtaz, D. W. Sullivan Jr and B. Fowler, *Handbook on the Toxicology of Metals*, Elsevier Academic Press, Netherlands, 2015.
24 S. I. S. Rattan, M. Kyriazis, S. A. Hofbrucker-MacKenzie, I. Sivaprakasam, Y. Ji and M. Manfred Kessels, *The Science of Hormesis in Health and Longevity*, Elsevier Academic Press, Netherlands, 2019.
25 R. Maurus, A. Begum, L. K. Williams, J. R. Fredriksen, R. Zhang, S. G. Withers and G. D. Brayer, *Biochemistry*, 2008, **47**, 3332–3344.
26 L. Ren, X. Qin, X. Cao, L. Wang, F. Bai, G. Bai and Y. Shen, *Protein Cell*, 2011, **2**, 827–836.
27 L. Phongphane, S. N. Mohd Radzuan, M. H. Abu Bakar, M. T. Che Omar, U. Supratman, D. Harneti, H. A. Wahab and M. N. Azmi, *Comput. Biol. Chem.*, 2023, **106**, 107938, DOI: **10.1016/j.compbiolchem.2023.107938**.
28 D. R. Roe and T. E. Cheatham III, *J. Chem. Theory Comput.*, 2013, **9**, 3084–3095.
29 C. Bouysset and S. Fiorucci, *J. Cheminf.*, 2021, **13**, 1–9.
30 Y. Fu, J. Zhao and Z. Chen, *Computational and Mathematical Methods in Medicine*, 2018, 3502514, DOI: **10.1155/2018/3502514**.
31 J. Lin, P. Wang, Z. Zhang, G. Xue, D. Zha, J. Wang, X. Xu and Z. Li, *Synth. Commun.*, 2020, **50**, 823–830.
32 A. Keivanloo, M. Bakherad and A. Rahimi, *Synthesis*, 2010, **10**, 1599–1602.
33 A. Keivanloo, M. Bakherad, F. Abbasi, T. Besharati-Seidani and A. H. Amin, *RSC Adv.*, 2016, **6**, 105433–105441.
34 J. H. Frederich, J. K. Matsui, R. O. Chang and P. G. Harran, *Tetrahedron Lett.*, 2013, **54**, 2645–2647.
35 M. H. A. Bakar, P. Y. Lee, M. N. Azmi, N. Syifa'Lotfiamir, M. S. F. Mohamad, N. S. N. Shahril, K. A. Shariff, H. Ya'akob, K. Awang and M. Litaudon, *Biocatal. Agric. Biotechnol.*, 2020, **25**, 101594, DOI: **10.1016/j.bcab.2020.101594**.
36 N. Mohamad, Y. H. Phua, M. H. A. Bakar, M. T. C. Omar, H. A. Wahab, U. Supratman, K. Awang and M. N. Azmi, *J. Mol. Struct.*, 2021, **1245**, 131007, DOI: **10.1016/j.molstruc.2021.131007**.
37 P. R. Arantes, M. D. Polêto, C. Pedebos and R. Ligabue-Braun, *J. Chem. Inf. Model.*, 2021, **61**, 4852–4856.